STUDY OF POSSIBLE PRECURSORS OF A SERIES OF SOLAR FLARES IN THE ACTIVE REGION OF NOAA 12230 ON DECEMBER 9, 2014

© 2025 G. G. Motorina[a,b,] *, I. N. Sharykin[b], I. V. Zimovets[b], A. S. Motorin[c]

[a]*Main (Pulkovo) Astronomical Observatory of the Russian Academy of Sciences, St. Petersburg, Russia.*

[b]*Institute for Space Research, Russian Academy of Sciences, Moscow, Russia.*

[c]*St. Petersburg National Research University of Information Technologies, Mechanics and Optics, St. Petersburg, Russia.*

**e-mail: g.motorina@yandex.ru*

Received February 25, 2025

Revised April 25, 2025

Accepted June 17, 2025

Abstract. The question of the nature of precursors of solar flares, as well as their relationship with subsequent flares, still has no unambiguous answer. This is due, in particular, to the lack of systematic statistical works, the relative incompleteness (in isolation from the context of the development of the entire active region) of studies of individual events, and the ambiguity of the term "precursor" itself. In this paper, we consider the dynamics of the NOAA 12230 active region (AR), in which a series of homologous outbursts (C5-C9) occurred on December 9, 2014 within 12 hours, with an average well of about 2 hours. This AO was characterized by a rapid increase in flare activity followed by a rapid decline, which can be considered as a good example to study potential precursors of flare series. We investigate the evolution of the NOAA 12230 AO over a relatively long period (several days) and its transition from the "no-flare" state to the flare-active regime. For this purpose, we study the magnetic field dynamics using SDO/HMI magnetograms, UV images from SDO/AIA data, and X-ray observations from GOES/XRS and RHESSI data. Thus, we have identified several phases of AR development in terms of magnetic field dynamics and burst/burst activity. We proposed a method for constructing hourly integral maps of UV variations (eclipses) from AIA 1600 Å data. We conclude that the significant increase in the chromospheric radiation variations against the background of a small flux of soft X-ray and UV radiation from the corona observed on December 8, 2014, together with the magnetic flux pop-up, can be regarded as a precursor to a series of flares. We also analyzed the appearance of X-ray sources of weak bursts before the series of flares. It is shown that the X-ray bursts developed in the same plasma structures where future flares would occur. The results obtained show the importance and prospects of applying new methods of synoptic observations of the Sun in the context of collecting statistics ("history") of AR energy release in different bands of the electromagnetic spectrum. In other words, it is important to monitor not only the dynamics of the magnetic field structure, but also how the

AO releases the stored magnetic energy. An integrated approach will make it possible to develop new methods for forecasting flares: perhaps better than just taking into account the magnetic field structure.

DOI: 10.31857/S00167940250721e7

1. INTRODUCTION

A precursor to a solar flare ("in the conventional sense") is commonly considered to be a localized small-scale energy release visible as a dimming in various wavelength ranges over a conventional time range from a few minutes to ~1-2 h before the main flare (e.g., [Wang et al., 2017]). Precursors can be both a manifestation of independent weaker episodes of energy release accompanying the evolution of the active region (AR) and a trigger for the main flare. In a broader sense, solar flare precursors can be understood as a wide variety of phenomena in the AO, indicating the instability of magnetic-plasma configurations. The problem of searching for precursors is closely related to the problem of accumulation and subsequent release of energy in ARs during solar flares, as well as to the applied problems of predicting powerful active phenomena on the Sun, including the prediction of space weather.

For example, in [Van Hoven and Hurford, 1986], the "classical" precursor to a flare and coronal mass ejection (CME) is described as the appearance of a burst of soft and hard X-ray radiation, indicating the preliminary heating of the plasma and acceleration of electrons before the main energy release of the flare. In addition, a spatial relationship between the small-scale energy release (precursor) near the neutral line (NL) of the magnetic field and the onset of the main flare was shown in [Wang et al., 2017]. At the same time, studies of radio and X-ray precursors [Chifor et al., 2007; Abramov-Maximov, Bakunina, 2022; Zimovets et al., 2022; Shohin et al., 2024; Motorina et al., 2023] showed that the sources of preflare fluctuations are usually localized in compact AO zones located near the NL not far (approximately within 20-30 angular seconds) from the sources of the main flare. This suggests that the small-scale energy release in the lower solar atmosphere may be associated with the onset of the main flare. Nevertheless, the question of precursors and their relation to the onset of solar flares is still open.

Note that not only X-ray and microwave bursts near flares, but also other morphological structures with different spatial scales and temporal dynamics in different ranges of the electromagnetic spectrum are considered as precursors of solar flares. The most striking manifestations of pre-flare activity are systematized in the list below:

1. Compact booms and bursts in different bands of the electromagnetic (EM) spectrum: in the ultraviolet (UV) and extreme ultraviolet (EUV) bands before solar flares [Chifor et al., 2006; Chifor

et al., 2007; Zimovets et al., 2022; Shohin et al., 2024] in the thermal soft X-ray range (e.g., [Chifor et al. 2006; Awasthi et al. 2014, 2018a, 2018b; Zhang et al., 2015; Zimovets et al., 2022]), gyrosynchrotron bursts of microwave radio emission [Kai et al., 1983; Wang et al., 2017; Bakunina et al., 2020a, 2020b];

2. Pre-flare hot channels visible in the AMC range [Cheng et al., 2014; Nindos et al., 2015; Hernandez-Perez et al., 2019; Sharykin et al., 2020];

3. Vertical lifting of magnetic loops and the eruptive magnetic harness prior to the onset of a solar flare and corresponding eruption [Ohyama and Shibata, 1997; Zhang et al., 2012; Zhang et al., 2015; Wu et al., 2016; Mitra et al., 2019];

4. Long-lived extended radiation sources in different ranges of the EM spectrum: e.g., radio sources above NLs (NLS - Neutral Line Sources, e.g., see [Uralov et al., 2008; Bakunina et al. [Uralov et al., 2008; Bakunina et al., 2015; Abramov-Maximov et al., 2015]) and sigmoids visible in the soft X-ray range [Gibson et al., 2002; Driel-Gesztelyi et al., 2015; Jiang et al., 2014];

5. Plasma currents found from UV/CUV spectroscopy and visual analysis of time-sequence images in the same wavelength range [Wallace et al., 2010, Dudik et al., 2016; Zhou et al., 2016; Woods et al., 2017; Huang et al., 2019];

6. Spectroscopy of various UV lines reveals their non-thermal broadenings and Doppler shifts, which can be associated with the activation of turbulent currents in pre-flare magnetic structures (e.g., [Jeffrey et al., 2018; Huang et al., 2019]);

7. Quasi-periodic pulsations in the pre-flare radiation fluxes (e.g., [Zhdanov & Charikov, 1985; Tan et al., 2016; Abramov-Maximov & Bakunina, 2022; Zimovets et al., 2022]) and oscillatory motions in the magnetic structures of pre-flare ARs [Zhou et al., 2016].

All these phenomena have been described in the vicinity (no more than 1-2 hours) of individual solar flares. However, from our point of view, it is of great interest to investigate on long (several days) time scales the complex of energy release phenomena in ARs before large series of flares, which can give a powerful integral effect in space weather. What is the nature of the behavior of radiation sources in different ranges of electromagnetic waves before a series of flares on long time scales of AR dynamics? What is the relationship between the dynamics of pre-flare radiation sources and the dynamics of the photospheric magnetic field in the AO?

The purpose of this work is to investigate a specially selected (see next section for selection criteria) NOAA AO 12230 in the time interval of its highest flare activity on December 9, 2014 (as well as about a day before and after) to search for precursors of a series of flares from multi-wavelength observations, including soft X-ray (GOES/XRS [White et al, 2005] and RHESSI [Lin et al., 2002]) and extreme ultraviolet (SDO/AIA, [Lemen et al., 2012]) emission, photospheric magnetic field data (SDO/HMI, [Scherrer et al., 2012]). In the present work, we attempt to highlight

characteristic processes in different spectral bands and in different layers of the solar atmosphere in ARs before a series of flares and discuss the possible nature of the occurrence of precursors.

From our point of view, the novelty of this work lies in the attempt to carry out a comprehensive multi-wavelength (magnetic field analysis + analysis of radiation from the chromosphere to the corona) study of the AO energy release before a series of solar flares on long time scales. We consider the activity "as a whole" for the selected AO and do not detail the analysis of individual events. It is worth noting that most modern works usually evaluate the peculiarities of the magnetic field dynamics in comparison with the soft X-ray fluxes by GOES and do not detail the statistics of the radiation sources during the evolution of ARs. We will collect statistics of radiation for a specific, selected AO in different ranges of the EM spectrum. Also, the novelty of this work lies in the selection and consideration of the remarkable case of AO NOAA 12230 (more details in the next section), which illustrates the evolution of the AO from a non-flare to a flare-active state and back in terms of simultaneous analysis of multi-wavelength observational and magnetic field data.

2. SELECTION OF AOS FOR ANALYSIS

For the analysis was chosen AO NOAA 12230, which appeared on the visible part of the Sun on December 6, 2014 (during the maximum of the 24th solar activity cycle), and in the process of development, starting from December 8, caused a series of solar flares X-ray class C. This AO was chosen to analyze the dynamics of flare activity in the UV and CUV bands due to the rapid growth of the spot group (within a day) and the appearance of a series of solar flares, with the 7 most powerful flares appearing within 12 hours. From our point of view, this AO is a remarkable object to study the features of the AO energy release before an isolated series of solar flares. In fact, it is difficult to find cases for large ARs (in which a series of powerful M- and X-class flares are observed) where we see the nucleation of an AR, followed by an active period and a decay of flare activity (see, e.g., [Fursyak et al., 2020; Nechaeva et al., 2024]). At the same time, we also need such an AO to be located in the central part of the solar disk in order to have acceptable quality of the HMI vector magnetograms. The chosen AO stands out because we can see its evolution from birth to the end of the flare-active period within about three days. At the same time, we have good vector magnetograms without the projection effect (characteristic of near-limb AOs). Also, relatively weak C-class flares did not produce strong oversaturation of the AIA matrix, which is also convenient for analyzing this AO. Based on the observations of this AO, we will collect unique information on the dynamics of radiation sources in different bands of the EM spectrum with respect to the dynamics of the photospheric magnetic field structure at different stages of AO development. In particular, we will emphasize the peculiarities of the AO transition to a series of flares.

3. OBSERVATIONAL DATA AND THEIR PROCESSING

The first flare occurred on December 8, 2014 at 17:53 UT (C1.3), followed on December 9, 2014 by a successive series of 11 flares from 03:21 UT (C2.0) to 23:22 UT (C1.3), and the last flare occurred on December 10, 2014 at 02:03 UT (C1.4), see Table 1. The flashes, X-ray class, start and end times are taken from the list freely available at the website: (https://umbra.nascom.nasa.gov/goes/eventlists/goes_event_listings_HER/). It should be noted that the flare that occurred on December 09, 2014 at 02:33 UT (C1.3) in NOAA AO 12230 (from goes_xray_event_list_2014) was not included in the list because it occurred on the western limb of the Sun and is not related to the AO in question. The duration between the end of one flare and the beginning of the next flare for December 09, 2014 ranged from 51 min to 3h. 30 min. The mean time between neighboring flashes was 100.0 min and the standard deviation was 50.4 min.

Figure 1 shows for December 08-10, 2014 the time profiles of X-ray emission from GOES data in channels 1-8, 0.5-4 Å, the CUF emission (94, 131 Å) from the region shown in Fig. 5, and the total variation of the UV emission (1600 Å) in AO NOAA 12230 in the 1600 Å channel from SDO/AIA data. The similarity of the temporal profiles of X-ray and UV emission (Fig. 1), which consisted of several peaks, is noteworthy.

To analyze the dynamics of the total magnetic field vector, we analyzed vector magnetograms of SDO/HMI. For further calculations, we took a fixed area that covered the entire AO. Figure 2 shows the time sequence of SDO/HMI magnetograms (Bz component maps after recalculation to spherical coordinates) for December 8 and 9, 2014. The time range of rapid formation of NOAA AO 12230 is clearly distinguished: ephemeral region (only Plage regions are visible) (a), appearance of regions of strong magnetic spot fields (b), relative divergence of spots and growth of their area (c, d). Vertical fields greater than ~1000 Gauss appeared during the appearance of the spots (see below for more details).

In Fig. 3. we analyze hourly integral (i.e., hourly summed) maps of UV brightening in the SDO/AIA 1600 Å channel (24 s temporal resolution). The field of view in the figure panels is not fixed and grows as the spots appear and the AR grows for better visualization. Summarized (i.e., integral) UV maps of urchins were constructed from the time sequence of SDO/AIA UV images as follows. NOAA 12230 AO difference images were compiled, and then pixels with negative time derivative were taken to be zero. Pixels in which the brightness growth per frame was less than 150 DNs/frame (DN - digital number) were also zeroed. Then at hourly intervals such difference maps (with pixels with significant brightness growth, i.e. more than 150 DNs/frame) were summed up and the value in each pixel was normalized by the number of frames in the selected hourly interval (~150 difference frames). Thus, maps of the integral hourly "positive" energy release were formed. On this basis, we compared the dynamics of chromospheric activity in the integral UV maps with

the averaged (for 1 hour) vector magnetograms (contours in Fig. 3): superimposition of the region of strong magnetic fields and drawing the position of the neutral line on the UV maps.

The four upper panels of Fig. 3 shows the appearance of spots (flux resurfacing) and the beginning of AR formation: a bipolar structure (~25 arc-sec) and the first compact UV brightenings with a characteristic size up to ~5 arc-sec appear. Probably, the first bores appear as a result of the interaction of the pop-up magnetic flux with the background magnetic field. We then observe a complication of the NL and the appearance of large-scale UV brightening regions: the most powerful outbursts are shown for 17:29:29:29 UT. For the 05:45:29 and 11:45:29 UT panels, we see a very strongly ruggedized NL and many UV brightenings near this NL. The last panel of Fig. 3 shows a point in time when we no longer see increased solar activity and the UV yarns become quite sparse and compact again.

In Fig. 4 shows different temporal profiles of the UV (1600 Å), CUF (131 Å), X-ray emission, and histograms of the distribution of the magnetic field vector components from SDO/HMI data. Panels (a) and (b) show the dynamics of the maximum (a, brightest map pixel) and total variation of the SDO/AIA 1600 Å UV emission at hourly summation (from the maps in Fig. 3). The total flux of 131 Å CUF emission from the studied AO is shown in panel d compared to the integrated flux from the whole Sun in the soft X-ray range (Fig. 4c) by GOES (channel 1-8 Å). When comparing the UV and X-ray light curves, it can be observed that the GOES data show bursts not only from the considered AO, but also from other regions of the Sun, which is important to take into account when studying flares and their precursors [Zimovets et al., 2022; Zimovets et al., 2023].

The dynamics of the histograms of the distribution of magnetic field components from SDO/HMI vector magnetograms (time resolution of 12 min) is shown in Fig. 4e-g: the modulus of the magnetic field vector (e), the modulus of the vertical (or radial, i.e., perpendicular to the Sun's surface at a given point) component (f), and the magnitude of the horizontal (or tangential, i.e., directed along the Sun's surface) component (g). The phase of magnetic flux surfacing and the formation of ARs with a group of spots from the ephemeral AR stage are clearly distinguished. The color scale qualitatively displays the total area of pixels with one or another field value (vertical scale) and by the purple color one can see that magnetic fields greater than ~700 Gauss (horizontal component) and ~1300 Gauss (vertical component) appear in the process of magnetic flux surfacing. The lower panels (h) and (i) show the magnetic fluxes computed for the vertical component over 1000 Gauss (h: negative and positive) and the time derivatives of these magnetic fluxes (i). These time profiles are compared with the total UV activity curve (b) and the total CUF 131 Å radiation flux for the studied AO (d).

The complex of observational data in Fig. 4 shows the presence of several phases in the development of the flare AO. In the first ephemeral phase, we observe only the diffuse field of the

flare plage (plage) and the NL, in the vicinity of which a local magnetic flux surfacing occurs, and the appearance of the first spots. The onset of the resurfacing corresponds to the first UV brightenings at the chromospheric level according to the AIA data: panel (h) shows in blue the histogram magnified by a factor of 10 in amplitude to see the weak increases (in the region of the first vertical dashed line). The maximum value of the magnetic flux variation for both signs of the vertical component of the magnetic field (second vertical line) is reached at the onset of the small-scale outburst coronal activity visible in the 131 Å AIA hot channel (as small outbursts compared to flares): the temporal profile in panel (i) with amplitude magnified by a factor of 5 is also shown for clarity. Also at this time point, we see the maximum value of the UV variations (from the hourly integral maps) in the curve in Fig. 4a and the beginning of strong integral chromospheric activity in the AO (Fig. 4h). The period of small-scale outburst activity ends with the beginning of a series of outbursts (between the third and fourth vertical line), after which the chromospheric activity disappears and the number of outbursts in the 131 Å channel decreases (after the fourth vertical line).

The analysis of the total maps of the UV brightenings and the magnetic field data indicates that these maps are sensitive to the magnetic field dynamics. The emergence of pinholes is associated with the surfacing of the magnetic flux and the complication of the magnetic field geometry (visible as the complication of the NL and the growth of a group of spots). It is likely that current layers forming in the corona above the AO and the energy release in them leads to energy fluxes from the corona to the chromosphere, and we see dynamic bright regions in the 1600 Å channel. The formation of current layers in the chromosphere is also possible in the case of low magnetic loops. Moreover, we note the important fact that after reaching the maximum rate of magnetic flux change, we begin to see very strong chromospheric activity and, after about 10 hours, the beginning of a series of flares whose chromospheric activity was comparable to the pre-flare period (with much stronger activity in the corona observed in the X-ray band).

To analyze the X-ray sources, images were constructed from RHESSI data in the 6-12 keV energy range (CLEAN algorithm, [Hurford et al., 2002]) for all visible outbursts in this AO prior to the C-class flare series on December 9, 2014. A comparison was made (Fig. 5) of the resulting X-ray contour images with the total hourly CUF maps of the 131 Å outbursts (similar to the UV outburst maps in Fig. 3). For a given channel, approximately 300 difference frames are stacked in the hourly time interval. In contrast to the UV total maps in the 1600 Å channel (predominantly chromospheric emission), the constructed maps in the 131 Å channel represent the integral hourly activity in the corona and should indicate the most heated magnetic-plasma configurations. In constructing the 131 Å summation maps, we summed the pixels of the difference images only for magnitudes of change greater than 300 DNs/frame (other pixels were zeroed). We compare the

summary maps and X-ray sources to the full magnetic field contours and do not show the NLs (to reduce the clutter in the figure; for the NLs and the vertical component of the magnetic field, see Fig. 3).

We plotted groups of X-ray sources for each individual burst within the considered hourly time interval of the total CUF maps (the beginning of hourly interval is shown in the captions above the panels in Fig. 5). Each individual X-ray source was constructed for sufficiently arbitrary time intervals so as to cover individual bursts or their groups in the time profiles of the RHESSI count rate in the 6-12 keV energy range, and also so that it was possible to synthesize an X-ray image from the data (to ensure convergence of the image reconstruction algorithm), given the rather poor statistics of the registered X-ray photons.

From Fig. 5 shows that X-ray sources and areas of increased CUF activity (bright green-red-yellow areas on the total CUF maps) are localized in the same region. At different hourly time intervals, the X-ray sources differ in size and magnitude of relative spread. The first "significant" C flare in the series is shown in panel (i). Panel (a) shows the hourly time interval in the vicinity of the maximum pre-flare burst of UV activity (when the third phase of pre-flare microburst activity began after the flux resurfacing phase). We see that an X-ray source arises between the paired regions of the CUF ejecta. A weak microburst was detected for this source ~ B1.0 if we subtract the background before this burst, which was at ~C1.0.

The analysis of the UV and CUV fluxes does not provide direct information on the plasma temperature in the AO. At the same time, one of the possible prognostic parameters of flare activity may be the average temperature in the AR, or its value in some localized places of the AR: for example, the temperature increase may indicate an increasing energy release in the pre-flare current layers. Within the framework of this work, we will perform a preliminary and simplest analysis of the thermodynamic parameters of the plasma in ARs in channels 94, 131, 171, 193, 211, 335 Å from SDO/AIA data and X-ray emission from GOES data. Using the AIA data, we recovered the differential emission measure (DEM) of the flash plasma along the beam of view from a region in the temperature range T = 0.5-25 MK to further determine the temperature (*T*) and emission measure (*EM*) from the FOV (field of view, Fig. 6, bottom panel) of the AO region of interest, assuming a multi-temperature model.

Using the AIA data with the Tikhonov regularization method [Tikhonov and Arsenin, 1979; Hannah and Kontar, 2012], we performed a reconstruction of the differential emission measure (DEM, Fig. 6, bottom panel). In Fig. 6 (bottom panel) shows the DEM calculated from the FOV (Fig. 6, top panel) for the most powerful flare SOL20141209T09:58 (C8.6) in the series for the time moments: 57 min before onset (09:00:47- 09:00:59 UT), at maximum (10:24:13-10:24:37 UT), and during the decline phase (10:35:00-10:35:12 UT). It can be seen that there are dynamics of DEM

development . There is an increase in the DEM, namely the part responsible for coronal plasma with temperatures above 5 MK, as the event progresses. This is most noticeable at the time of the maximum of the impulsive phase (10:24:13-10:24:37 UT). The flare-associated heating and growth of the emission measure can be seen in Fig. 7.

The resulting time profiles of temperature and emission measure from GOES and AIA data for a long (~20 h) time interval are shown in Fig. 7. It can be seen that there is a correlation between the *EM* and *T* profiles. Moreover, *EM* and *T* do not show such a clear variation as the temporal profiles of the CUF emission, which can be explained by the fact that *EM* and *T* are integral features. It can also be noted that the variations in the amplitude of *EM* and *T* by AIA are weaker than the variations of *EM* and *T* by GOES due to the fact that for AIA the analysis was performed for a selected region of the Sun (recall that GOES measures the integral X-ray fluxes from the entire visible hemisphere of the Sun), and also AIA is sensitive to lower temperatures of the emitting plasma compared to GOES [Tsap and Motorina, 2017].

4. DISCUSSION OF RESULTS AND CONCLUSIONS

We analyzed the time sequence of UV and CUV images (chromospheric and coronal emission) from 1600 and 131 Å AIA data of the NOAA 12230 active region before and during the outburst activity on December 8-9, 2014, in order to identify the features of the active region preparation for a series of outbursts of 11 X-ray class C events with a mean time between them of 100± 50 min. A simple efficient method (integral hourly UV and CUF maps of the positive intensity derivative) for visualizing the brightenings in the chromosphere and corona was proposed and demonstrated using a selected AO that best shows the nucleation of the spot group, the transition to the flare series, and the fading of the flare activity.

It is shown that the method of UV chromospheric brightening maps is very sensitive to changes (magnetic flux pop-up and NL complexity) in the photospheric magnetic field. It is likely that this method of mapping the variations of energy release in the AO at the chromospheric level can be used as an additional source of information on the status of energy release in the AO to create new solar flare prediction models (along with information on the photospheric magnetic field). However, extensive statistical work is needed to create such a method. In this paper, we have only demonstrated an example of simultaneous qualitative analysis of data on the photospheric magnetic field, total maps of UV chromospheric activity, and integral coronal CUF flux for a specific selected AR.

The main physical conclusion of this work is to distinguish the phases of AO preparation for a series of flares. Moreover, the possibility of obtaining this result is due to the fact that we have chosen an ideally suited fast evolving AO to study and different types of data showing different layers of the solar atmosphere. In particular, the method of total UV chromospheric maps allowed

us to identify a phase of enhanced chromospheric activity before a series of flares. As a result, five developmental phases were identified for the studied AR from its nucleation to the cessation of flare activity. The boundaries between the phases and their names are rather conventional:

- Phase 1. "Ephemeral AO" without spots (only flare site areas);

- Phase 2 ("Photospheric" phase, birth of AO). Beginning of magnetic flux surfacing. Formation of pores and small spots. First UV brightenings appear in very compact areas. In this phase, the fluxes of the CUF radiation in the 131 Å channel gradually change, and bursts are not yet observed;

- Phase 3 ("Chromospheric phase" against the background of small bursts of CUF radiation). Beginning of microburst coronal activity: probably precursors of future flare activity. This phase is observed from a very bright burst at 1600 Å, but with a weak manifestation in the corona (probably very low magnetic loops are involved). The UV brightenings become very bright and cover a large area. Bursts in the 131 Å hot channel begin to be observed. Here we observe the first X-ray microburst at ~B1.0 (taking into account the subtracted background). This phase is associated with the formation of a complex NL, probably related to the secondary flaring of the compact magnetic flux against the background of the forming AR;

- Phase 4 ("Coronal Flare Phase"). Flash activity in the form of a continuous series of C flares. A complex morphology of radiation sources is observed. The cause of the flares is clearly related to the complex NL and magnetic field geometry;

- Phase 5 ("Fading of flare activity" in all bands of the EM spectrum). Attenuation of flare activity and AO exit to the stationary regime. The AO then moves through the disk as an AO that has a Hale class (or Mount Wilson class) of βγ (see e.g., [Toriumi and Wang, 2019]).

We consider X-ray microbursts and weak flares (B to C class) in the context of the development of the NOAA 12230 AO from its very inception to the onset of flare activity. The complex of observational multi-wavelength data suggests that the location of X-ray sources prior to the C series of flares is associated with a heated magneto-plasma structure (visible in the total CUF maps) in which the energy release of future flares of this AO will develop. Despite the apparent obviousness of this statement, we note that, from our point of view, there has been insufficient real end-to-end analysis of the dynamics of X-ray flare sources (of different powers) over relatively long time intervals. Usually, studies of the Sun's X-ray emission are tied to specific (more often large over M1.0 class) events. In this paper, we have shown by comparing total CUF variation maps, HMI vector magnetograms, and X-ray images that X-ray activity in ARs is localized in the corona above the NL between spots, where the energy release of a series of flares occurs. We note that the importance of processes over the NL prior to flares has been noted in numerous papers (some of them mentioned in the Introduction): mostly analyzing single events and time moments near the

onset of flares. In this paper, we have strengthened the assertion of the importance of diagnosing high-energy processes in the AO over NLs by analyzing processes in the AO over long time intervals. This simple result is important precisely from the point of view of solar flare prediction practice: collecting information on the real status of the AO energy release in the X-ray range (as well as in other ranges of the EM spectrum) in the context of the magnetic field dynamics. In other words, it is important not only the "AO energy content" (the value of free magnetic energy), but also how the AO releases magnetic energy in the form of flares and small bursts of different energy scales.

In addition to analyzing maps and images, it seems important to construct averaged characteristics of the CUF radiation by DEM analysis. Again because of the importance of tracking the current status of the AO energy emission. In this work, we analyze the differential emission measure and calculate the flash plasma parameters (T, EM). It is shown that there is a good correlation between the emission measure and temperature profiles obtained from GOES and AIA data, indicating a single process observed with both instruments. A comparison of the AIA coronal channels and GOES data confirmed the presence of outbursts from another AO in the X-ray data. The method of using DEM analysis of AOs in the context of developing forecasting methods needs to be further developed. Here, we investigated the simplest parameters from the integral DEM AO FOV with the aim of further developing prognostic criteria from XRF data.

The consideration of precursors 1-2 h before the flare onset very strongly limits the realistic possibilities of predicting the AO energy release against the background of slower magnetic field dynamics. This work has shown that it is necessary to consider long time periods of AR development and also to monitor the integral energy release in ARs. In particular, before the beginning of the flare series on December 9, 2014, the studied AO showed a significant enhancement of the chromospheric UV flux in about 12 hours (Fig. 4), which can be considered as a precursor of the flare series against the background of the magnetic field resurfacing. In other words, the pumping of ARs with magnetic energy followed first, and then the formation of unsteady magnetic configurations and, in particular, current layers occurred. With this approach to data analysis, the concept of a precursor (as a concept for practical flare prediction problems) in a few minutes or tens of minutes loses its meaning. However, these statements require additional analysis of the observations. Extensive statistical work must be done to put into practice the forecast of flares based on observations of energy release in ARs.

It is worth noting that virtually all past and present studies of microflares have been conducted in the context of coronal heating studies or as detailed multi-wavelength studies of individual events. In this work, we have shown that the energy release in the form of relatively weak bursts of radiation in the developing AR is related to the future energy release of solar flares. The implication

is that small acts of energy release are indicative of growing instability and future flares.

Once again, we emphasize the main methodological conclusion of this paper. We have demonstrated a qualitative approach to the analysis of multi-wavelength observational data of a particular flare AO and have shown the possibility of collecting (by constructing total UV and CUV maps and DEM analysis) information on activity of different energy scales in the context of the photospheric magnetic field dynamics. Further it is necessary to proceed to statistical studies, elaboration of methods and development of quantitative parameters indicating the conditional current and previous (relative to a given point in time) status of the AO energy release in order to forecast future energy release using also magnetic field data. From our point of view, progress in empirical models of solar activity prediction will be related to the addition of additional data on EM radiation from the overlying layers of the solar atmosphere with sufficiently good spatial resolution to the usual used vector magnetograms.

FUNDING

This work was supported by RNF grant 20-72-10158.

CONFLICT OF INTERESTS

The authors declare that they have no conflicts of interest.

REFERENCES

1. *Tikhonov A.N., Arsenin V.Ya.* Methods for solving ill-posed problems. Moscow: Nauka, 286 p. 1979.
2. *– Abramov-Maximov V.E., Borovik V.N., Opeikina L.V., et al.* Precursors of the solar X flare on march 29, 2014, in the active region NOAA 12017 based on microwave radiation and magnetographic data // Sol. Phys. 290. 53. 2015.
3. *Abramov-Maximov V.E., Bakunina I.A.* Signs of preparation of solar flares in the microwave range // Ge&Ae. V. 62. No. 7. P. 895–902. 2022.
4. *Awasthi A.K., Jain R., Gadhiya P.D., et al.* Multiwavelength diagnostics of the precursor and main phases of an M1.8 flare on 2011 April 22 // MNRAS. V. 437. I. 3. 2249. 2014.
5. *Awasthi A.K., Liu R., Wang H., et al.* Pre-eruptive magnetic reconnection within a multi-flux-rope system in the solar corona // Astrophys. J. V. 857. I. 2. 124. 2018a.
6. *Awasthi A.K., Rudawy P., Falewicz R., et al.* Chromospheric response during the precursor and the main phase of a B6.4 flare on 2005 August 20 // Astrophys. J. V. 858. I. 2. 98. 2018b.
7. *Bakunina I.A., Melnikov V.F., Morgachev A.S.* Preflare dynamics of microwave and ultraviolet emission in active regions of the Sun // Astrophysics. V. 63. I. 2. 252. 2020a.
8. *Bakunina I.A., Melnikov V.F., Morgachev A.S.* Signs of preflare situation in solar ultraviolet

and microwave emission // Ge&Ae. V. 60. I. 7. 853. 2020b.

9. *Bakunina I.A., Melnikov V.F., Solov'ev A.A., et al.* Intersunspot microwave sources // Sol. Phys. V. 290. I. 1. 37. 2015.
10. *Cheng X., Ding M.D., Zhang J., et al.* On the relationship between a hot-channel-like solar magnetic flux rope and its embedded prominence // Astrophys. J. V. 789. I. 2. L35. 2014.
11. *Chifor C., Mason H.E., Tripathi D., et al.* The early phases of a solar prominence eruption and associated flare: a multi-wavelength analysis // Astron. and Astrophys. V. 458. I. 3. 965. 2006.
12. *Chifor C., Tripathi D., Mason H.E., et al.* X-ray precursors to flares and filament eruptions // Astron. and Astrophys. V. 472. I. 3. 967. 2007.
13. *Dudík J., Polito V., Janvier M., et al.* Slipping magnetic reconnection, chromospheric evaporation, implosion, and precursors in the 2014 September 10 X1.6-class solar flare // Astrophys. J. V. 823. I. 1. 41. 2016.
14. *Fursyak Yu.A., Abramenko V.I., Kutsenko A.S.* Dynamics of electric current's parameters in active regions on the Sun and their relation to the flare index // Astrophysics. V. 63. I. 2. 2020.
15. *Gibson S.E., Fletcher L., Del Zanna G., et al.* The structure and evolution of a sigmoidal active region // Astrophys. J. V. 574. I. 2. 1021. 2002.
16. *Hannah I.G., Kontar E.P.* Differential emission measures from the regularized inversion of Hinode and SDO data // A&A. V. 539. Id. A146. P. 14. 2012.
17. *Hernandez-Perez A., Su Y., Thalmann J., et al.* A hot cusp-shaped confined solar flare // Astrophys. J. V. 887. I. 2. L28. 2019.
18. *Huang N., Xu Y., Sadykov V.M., et al.* Spectral Diagnosis of Mg II and Hα Lines during the Initial Stage of an M6.5 Solar Flare // Astrophys. J. V. 878. I. 1. L15. 2019.
19. *Hurford G.J., Schmahl E.J., Schwartz R.A., et al.* The RHESSI imaging concept // Sol. Phys. V. 210. I. 61. 2002.
20. *Jeffrey N.L.S., Fletcher L., Labrosse N., et al.* The development of lower-atmosphere turbulence early in a solar flare // Science Advances. V.4. I. 12. 2794. 2018.
21. *Jiang C., Wu S.T., Feng X., et al.* Formation and eruption of an active region sigmoid. I. A study by nonlinear force-free field modeling // Astrophys. J. V.780. 55. 2014.
22. *Kai K., Nakajima H., and Kosugi T.* Radio observations of small activity prior to main energy release in solar flares // Publ. Astron. Soc. Japan. V. 35. I. 2. 285. 1983.
23. *Lemen J.R., Title A.M., Akin D.J. et al.* The Atmospheric Imaging Assembly (AIA) on the Solar Dynamics Observatory (SDO) // Sol. Phys. V. 275. I. 1-2. P. 17-40. 2012.
24. *Lin R.P., Dennis B.R., Hurford G.J., et al.* The Reuven Ramaty High-Energy Solar

Spectroscopic Imager (RHESSI) // Sol. Phys. V. 210. I. 1. P. 3–32. 2002.

25. *Mitra P.K. and Joshi B.* Preflare processes, flux rope activation, large-scale eruption, and associated X-class flare from the active region NOAA 11875 // Astrophys. J. V. 884. 46. 2019.
26. *Motorina G.G., Tsap Yu.T., Smirnova V.V., et al.* Pre-impulsive and impulsive phases of the sub-terahertz flare of March 28, 2022 // Ge&Ae. V. 63. I. 8. p.1218-1223. 2023.
27. *Nechaeva A.B., Zimovets I.V., Zubik V.S., et al.* Evolution of characteristics of vertical electric current and magnetic field in active regions of the Sun and their relation to powerful flares // Ge&Ae. V. 64. I. 2. p. 150-171. 2024.
28. *Nindos A., Patsourakos S., Vourlidas A., et al.* How common are hot magnetic flux ropes in the low solar corona? A statistical study of EUV observations // Astrophys. J. V. 808. 2. 117. 2015.
29. *Ohyama M. and Shibata K.* Preflare heating and mass motion in a solar flare associated with hot plasma ejection: 1993 November 11 C9.7 flare // Publ. Astron. Soc. Japan. 49. 249. 1997.
30. *Scherrer P.H., Schou J., Bush R.I., et al.* The Helioseismic and Magnetic Imager (HMI) investigation for the Solar Dynamics Observatory (SDO) // Sol. Phys. V. 275. I. 1-2. 207. 2012.
31. *Sharykin I.N., Zimovets I.V., and Myshyakov I.I.* Flare energy release at the magnetic field polarity inversion line during the M1.2 solar flare of 2015 March 15. II. Investigation of photospheric electric current and magnetic field variations using HMI 135 s vector magnetograms // Astrophys. J. V. 893. I. 2. 159. 2020.
32. *Shohin T.D., Charikov Yu.E., Shabalin A.N.* Ultraviolet and X-ray precursors of solar flares // Ge&Ae. V. 64. I. 8. p. 1386-1394. 2024.
33. *Tan B., Yu Z., Huang J., et al.* Very long-period pulsations before the onset of solar flares // Astrophys. J. V. 833. I. 2. 206. 2016.
34. *Toriumi S., Wang H. Flare*-productive active regions // Living Rev. Sol. Phys. V. 16. 3. 2019.
35. *Tsap Yu.T., Motorina G.G.* Flare plasma diagnostics from X-Ray and Ultraviolet observations // Ge&Ae. V. 57. I. 7. 2017.
36. *Uralov A.M., Grechnev V.V., Rudenko G.V., et al.* Microwave neutral line associated source and a current sheet // Sol. Phys. V. 249. I. 2. 315. 2008.
37. *Van Driel-Gesztelyi L. and Green L.M.* Evolution of active regions // Living Rev. Sol. Phys. V. 12. I. 1. 2015.
38. *Van Hoven G., Hurford G.J.* Solar flare precursors // ASR. V. 6. I. 6. 1986.

39. *Wallace A.J., Harra L.K., Van Driel-Gesztelyi L., et al.* Pre-flare flows in the corona // Sol. Phys. V. 267. I. 2. 2010.
40. *Wang H., Liu C., Ahn K., et al.* High-resolution observations of flare precursors in the low solar atmosphere // Nature Astronomy. V. 1. 0085. 2017.
41. *White S.M., Thomas R.J., Schwartz R.A.* Updated expressions for determining temperatures and emission measures from Goes soft X-ray measurements // Sol. Phys. V. 227. I. 2. 231. 2005.
42. *Woods M.M., Harra L.K., Matthews S.A., et al.* Observations and modelling of the pre-flare period of the 29 March 2014 X1 flare // Sol. Phys. V. 292. I. 2. 38. 2017.
43. *Wu Z., Chen Y., Huang G., et al.* Microwave imaging of a hot flux rope structure during the pre-impulsive stage of an eruptive M7.7 solar flare // Astrophys. J. V. 820. I. 2. L29. 2016.
44. *Zhang J., Cheng X., and Ding M.-D.* Observation of an evolving magnetic flux rope before and during a solar eruption // Nature Communications. V. 3. Id. 747. 2012.
45. *Zhang Y., Tan B., Karlicky M., et al.* Solar radio bursts with spectral fine structures in preflares // Astrophys. J. V. 799. I. 1. Id. 30. 2015.
46. *Zhdanov A.A., Charikov Y.E.* Power spectrum analysis of preflare solar X-rays // Soviet Astronomy Letters. V.11. 88. 1985.
47. *Zhou G.P., Zhang J., and Wang J.X.* Observations of magnetic flux-rope oscillation during the precursor phase of a solar eruption // Astrophys. J. L. V. 823. I. 1. L19. 2016.
48. *Zimovets I.V., Nechaeva A. B., Sharykin I.N., et al.* Sources of long-period X-ray pulsations before the onset of solar flares // Ge&Ae. V. 62. I.4. 356. 2022.
49. *Zimovets I.V., Sharykin I.N., Kaltman T.I., et al.* Preflare X-ray pulsations with sources outside the main flare active region // Ge&Ae. V.63. I.5. 513. 2023.

Table. List of solar flares that occurred between December 8 and 10, 2014 in NOAA AO 12230. From left to right: date, start time, maximum, end of flare, GOES X-ray class, and time between the end of one flare and the beginning of the next.

Date	Start time	Peak time	End time	X-Class	Time between flares
8-Dec-2014	17:53	17:56	18:00	C1.3	-
9-Dec-2014	03:21	03:28	03:47	C2.0	
9-Dec-2014	04:56	05:15	05:39	C1.4	1 h. 9 min.
9-Dec-2014	08:22	08:30	08:41	C8.1	2 h. 43 min.
9-Dec-2014	09:58	10:24	10:35	C8.6	1 h. 17 min.

9-Dec-2014	12:29	12:34	12:45	C5.4	1 h. 54 min.
9-Dec-2014	13:43	13:48	13:56	C4.5	58 min.
9-Dec-2014	15:21	15:28	15:33	C6.2	1 h. 25 min.
9-Dec-2014	17:12	17:18	17:23	C2.5	1 h. 39 min.
9-Dec-2014	18:37	18:48	18:55	C5.3	1 h. 14 min.
9-Dec-2014	19:46	19:49	19:52	C1.4	51 min.
9-Dec-2014	23:22	23:27	23:32	C1.3	3 h. 30 min.
10-Dec-2014	02:03	02:13	02:21	C1.4	-

FIGURE CAPTIONS

Fig. 1. Time profiles at the time instant of December 8-10, 2014 of the GOES X-ray flux in channels 1-8, 0.5-4 Å (upper panel), the CUF flux in AO in SDO/AIA channels 94, 131 Å, and the total variation of the UV emission (in rms) in AO in channel 1600 Å (lower panel). The vertical lines show the beginning and end of the flashes.

Fig. 2. Time sequence of SDO/HMI magnetograms for NOAA AO 12230: maps of the Bz component at the time points (left to right from top to bottom): 08.12.2014 10:59:59:52 UT, 08.12.2014 13:59:52 UT, 09.12.2014 01:59:52 UT, 09.12.2014 21:59:52 UT.

Fig. 3. Time sequences of the integral (averaged) UV maps of ullages (colored substrate) in the SDO/AIA 1600 Å channel. These maps were made by summing in hourly time intervals all positive time derivatives (in pixels). The white contours show the magnetic field modulus levels (500, 1000, and 1500 Gauss). The bold line shows the position of the NL.

Fig. 4. Time profiles: maximum UV variation level (brightest pixel in the UV maps) in the NOAA 12230 AO in the 1600 Å channel (a), total UV variation in the NOAA 12230 AO in the 1600 Å channel (b), GOES X-ray flux in the 1-8 Å channel (c), CUF flux in the 131 Å channel (d), histograms of the magnetic field component distribution (X axis shows time and Y axis shows histogram): field modulus (e), modulus Bz component (f), horizontal B component (g). The color scale of the histograms shows the logarithm of the total area of the regions (in cm^2) for a particular value of the magnetic field component magnitude (marked on the vertical axis). The vertical lines mark the characteristic stages of the NOAA 12230 AO and background energy release. The panels (h, i) show the amplitude-increased temporal profiles of the UV emission in the 1600 Å channel and the CUF emission in the 131 Å channel (blue) for better visualization of weak bursts.

Fig. 5. RHESSI images of 6-12 keV X-ray emission sources (detectors 3, 6, 7). Time sequences of the CUF maps of ejecta (colored substrate) in the 131 Å channel. White contours show the magnetic field modulus levels (500, 1000, 1500, and 2000 Gauss). The cyan contours show the positions of the sources in the energy range 6-12 keV.

Fig. 6. Upper panel: analyzed region (FOV) of NOAA AO 12230, 09:00:49 UT 09.12.2014. Bottom panel: DEM calculated from the FOV for three time points: 57 min before the SOL20141209T09:58 (C8.6) flare onset (09:00:47-09:00:59 UT), at maximum of the impulsive phase (10:24:13-10:24:37 UT), and during the decline phase (10:35:00-10:35:12 UT).

Fig. 7. Left: temporal evolution of temperature (*T*) and emission measure (*EM*) calculated from GOES and SDO/AIA data from the region shown in Fig. 6 (left panel). Right: light curves of the CUV emission from the FOV (see Fig. 6), December 9, 2014. The vertical lines show the

beginning and end of the flares.

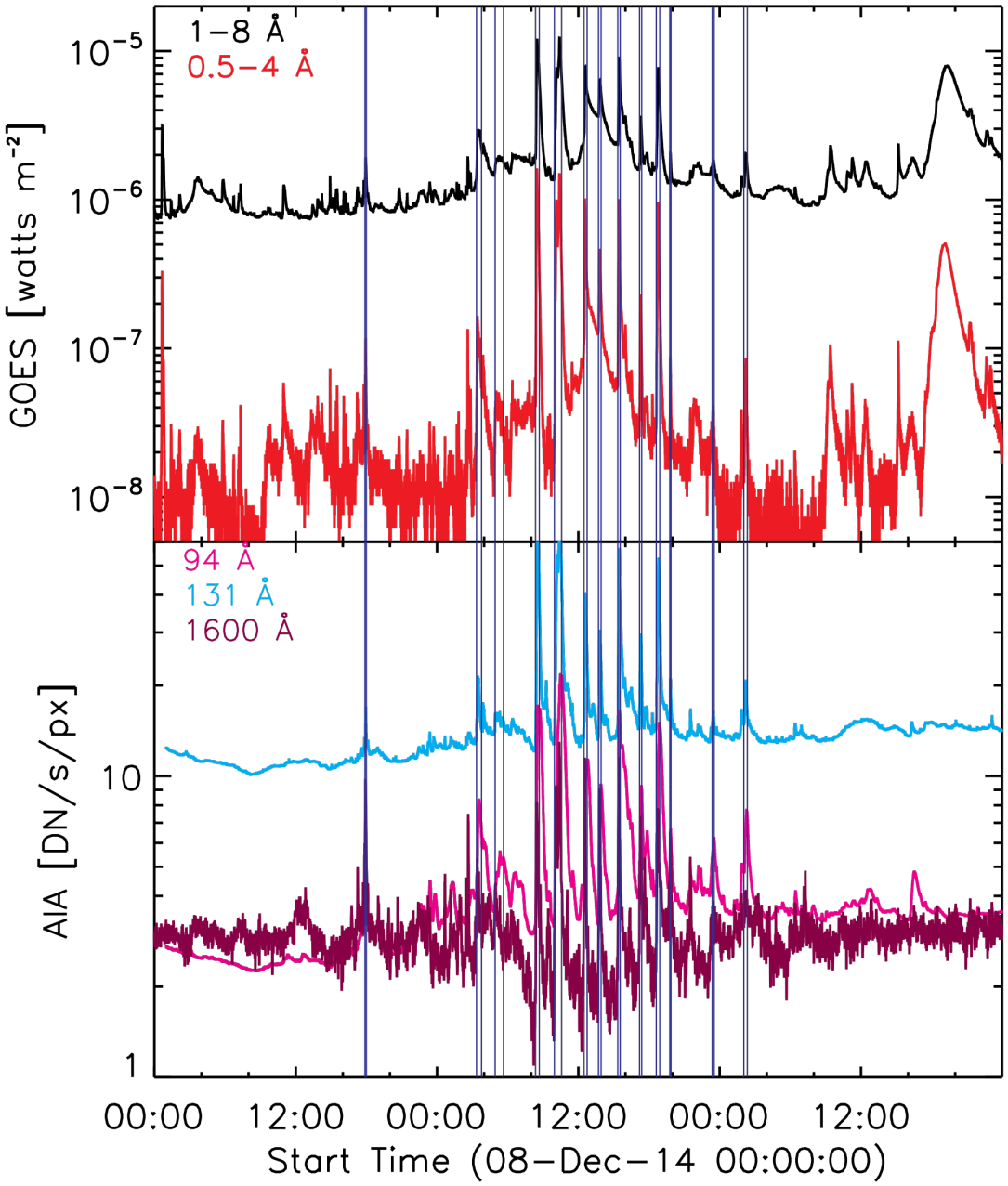

Fig. 1.

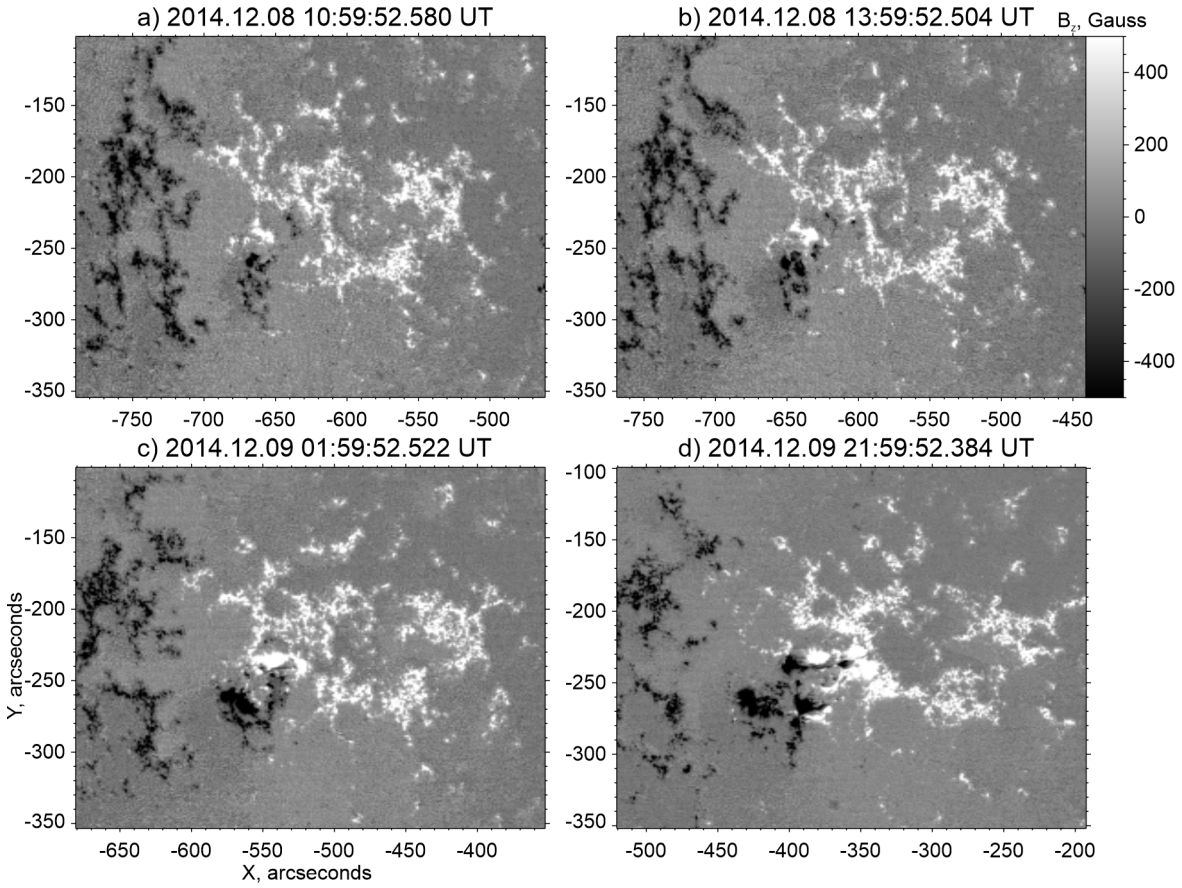
a) 2014.12.08 10:59:52.580 UT
b) 2014.12.08 13:59:52.504 UT
B_z, Gauss
400
200
0
-200
-400
c) 2014.12.09 01:59:52.522 UT
d) 2014.12.09 21:59:52.384 UT
Y, arcseconds
X, arcseconds

Fig. 2.

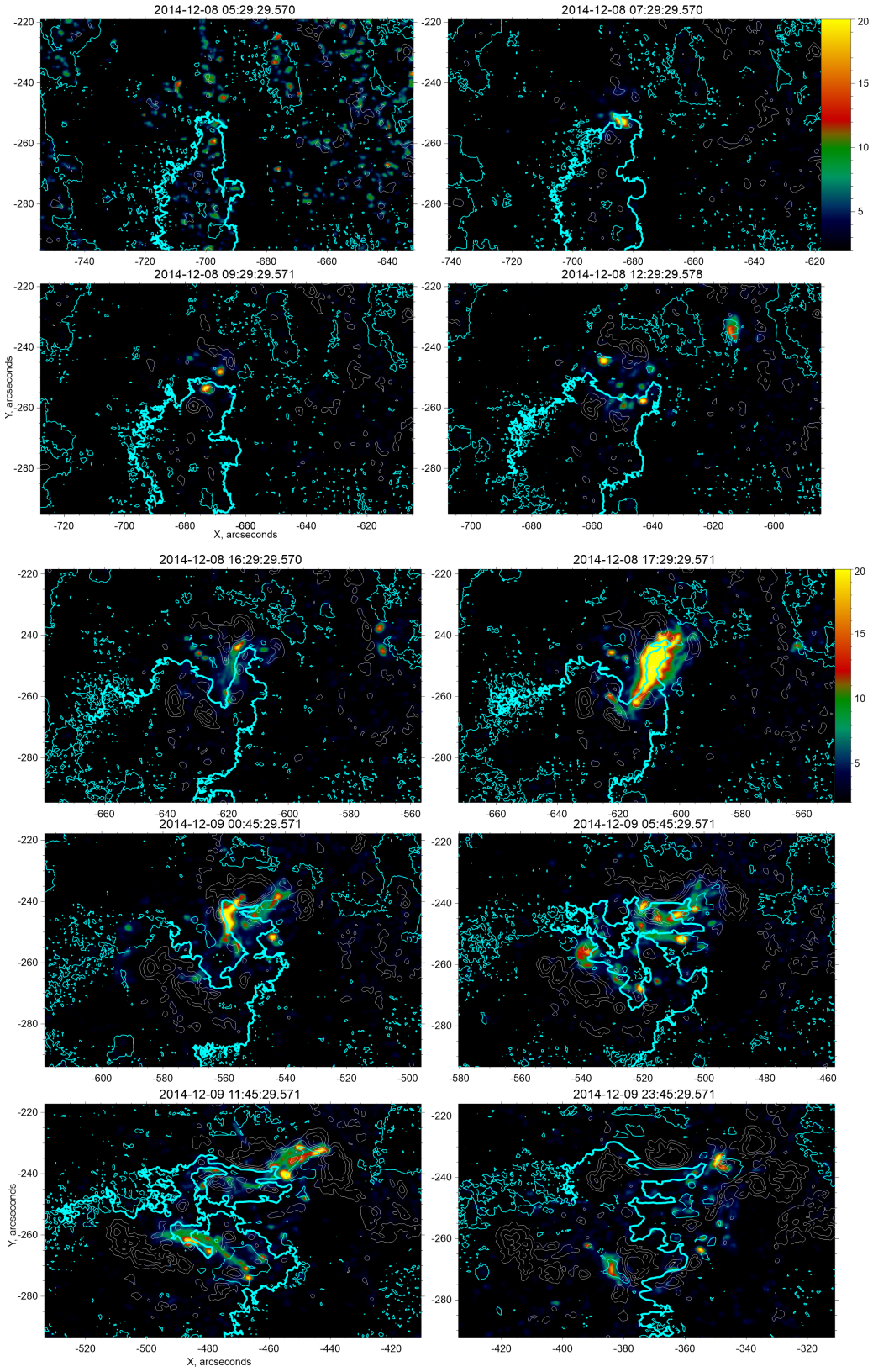
2014-12-08 05:29:29.570
2014-12-08 07:29:29.570
2014-12-08 09:29:29.571
2014-12-08 12:29:29.578
2014-12-08 16:29:29.570
2014-12-08 17:29:29.571
2014-12-09 00:45:29.571
2014-12-09 05:45:29.571
2014-12-09 11:45:29.571
2014-12-09 23:45:29.571
Y, arcseconds
X, arcseconds

Fig. 3.

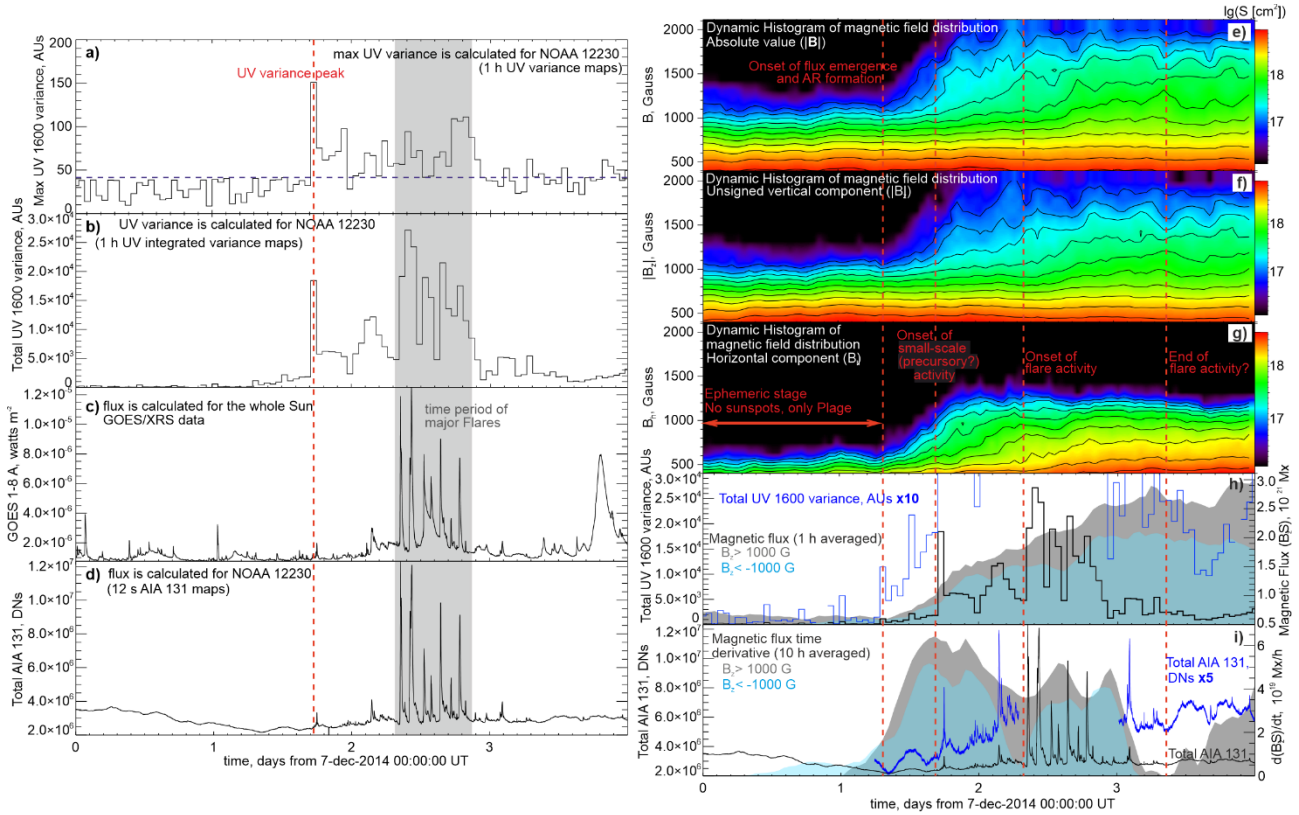
a)
max UV variance is calculated for NOAA 12230
(1 h UV variance maps)
UV variance peak
Max UV 1600 variance, AUs
b)
UV variance is calculated for NOAA 12230
(1 h UV integrated variance maps)
Total UV 1600 variance, AUs
c) flux is calculated for the whole Sun
GOES/XRS data
time period of
major Flares
GOES 1-8 A, watts m²
d) flux is calculated for NOAA 12230,
(12 s AIA 131 maps)
Total AIA 131, DNs
time, days from 7-dec-2014 00:00:00 UT
lg(S [cm²])
Dynamic Histogram of magnetic field distribution
Absolute value (|B|)
Onset of flux emergence
and AR formation
e)
B, Gauss
Dynamic Histogram of magnetic field distribution
Unsigned vertical component (|B|)
f)
|B_L|, Gauss
Dynamic Histogram of
magnetic field distribution
Horizontal component (B_L)
Onset of
small-scale
(precursory?)
activity
Onset of
flare activity
End of
flare activity?
Ephemeric stage
No sunspots, only Plage
g)
B_L, Gauss
Total UV 1600 variance, AUs x10
Magnetic flux (1 h averaged)
B_z > 1000 G
B_z < -1000 G
h)
Magnetic Flux (BS), 10²¹ Mx
Magnetic flux time
derivative (10 h averaged)
B_z > 1000 G
B_z < -1000 G
Total AIA 131,
DNs x5
i)
d(BS)/dt, 10¹⁸ Mx/h
Total AIA 131
time, days from 7-dec-2014 00:00:00 UT

Fig. 4.

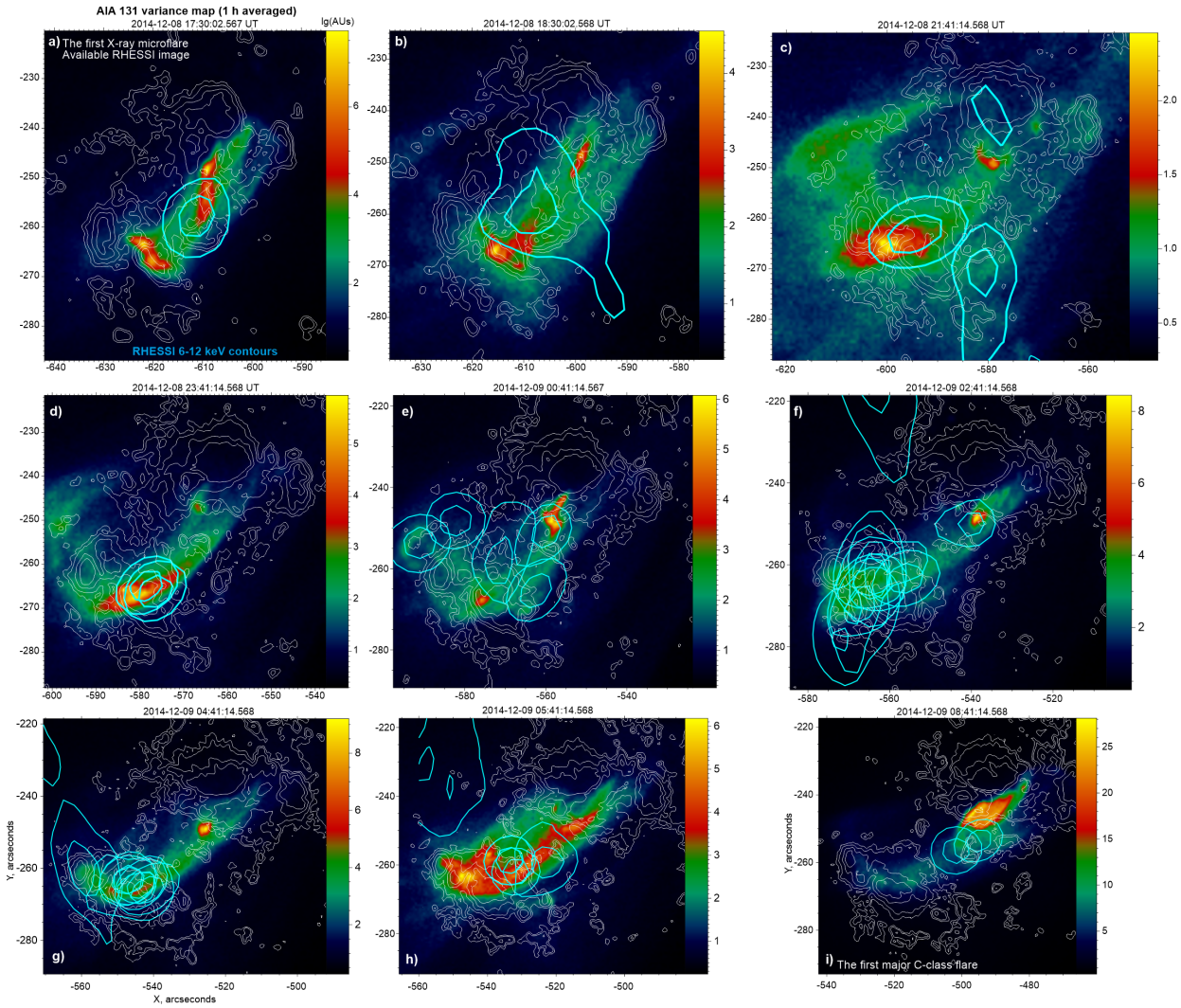
AIA 131 variance map (1 h averaged)
2014-12-08 17:30:02.567 UT
lg(AUs)
a) The first X-ray microflare
Available RHESSI image
RHESSI 6-12 keV contours
2014-12-08 18:30:02.568 UT
b)
2014-12-08 21:41:14.568 UT
c)
2014-12-08 23:41:14.568 UT
d)
2014-12-09 00:41:14.567
e)
2014-12-09 02:41:14.568
f)
2014-12-09 04:41:14.568
g)
2014-12-09 05:41:14.568
h)
2014-12-09 08:41:14.568
i) The first major C-class flare
Y, arcseconds
X, arcseconds

Fig. 5.

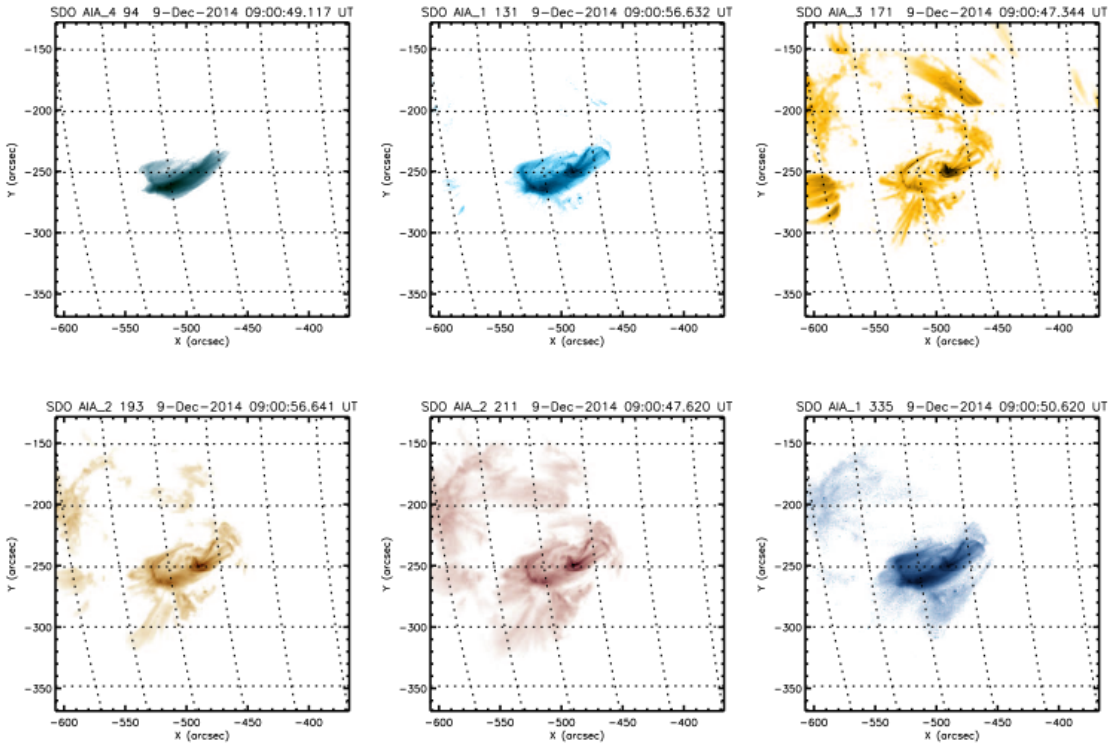
SDO AIA_4 94 9-Dec-2014 09:00:49.117 UT
SDO AIA_1 131 9-Dec-2014 09:00:56.632 UT
SDO AIA_3 171 9-Dec-2014 09:00:47.344 UT
SDO AIA_2 193 9-Dec-2014 09:00:56.641 UT
SDO AIA_2 211 9-Dec-2014 09:00:47.620 UT
SDO AIA_1 335 9-Dec-2014 09:00:50.620 UT
Y (arcsec)
X (arcsec)

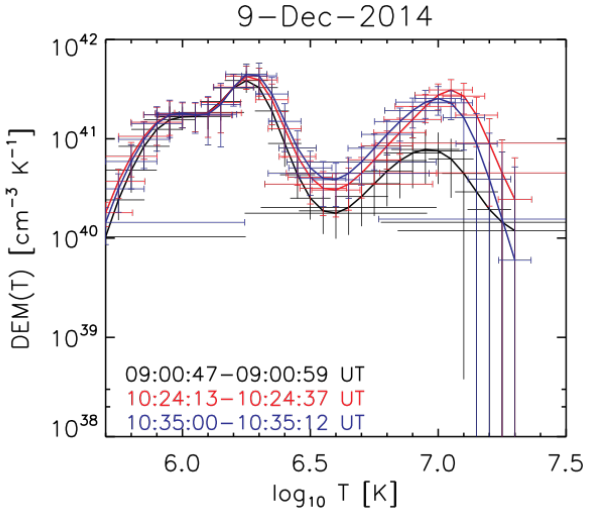
9-Dec-2014
DEM(T) [cm^{-3} K^{-1}]
log$_{10}$ T [K]
09:00:47-09:00:59 UT
10:24:13-10:24:37 UT
10:35:00-10:35:12 UT

Fig. 6.

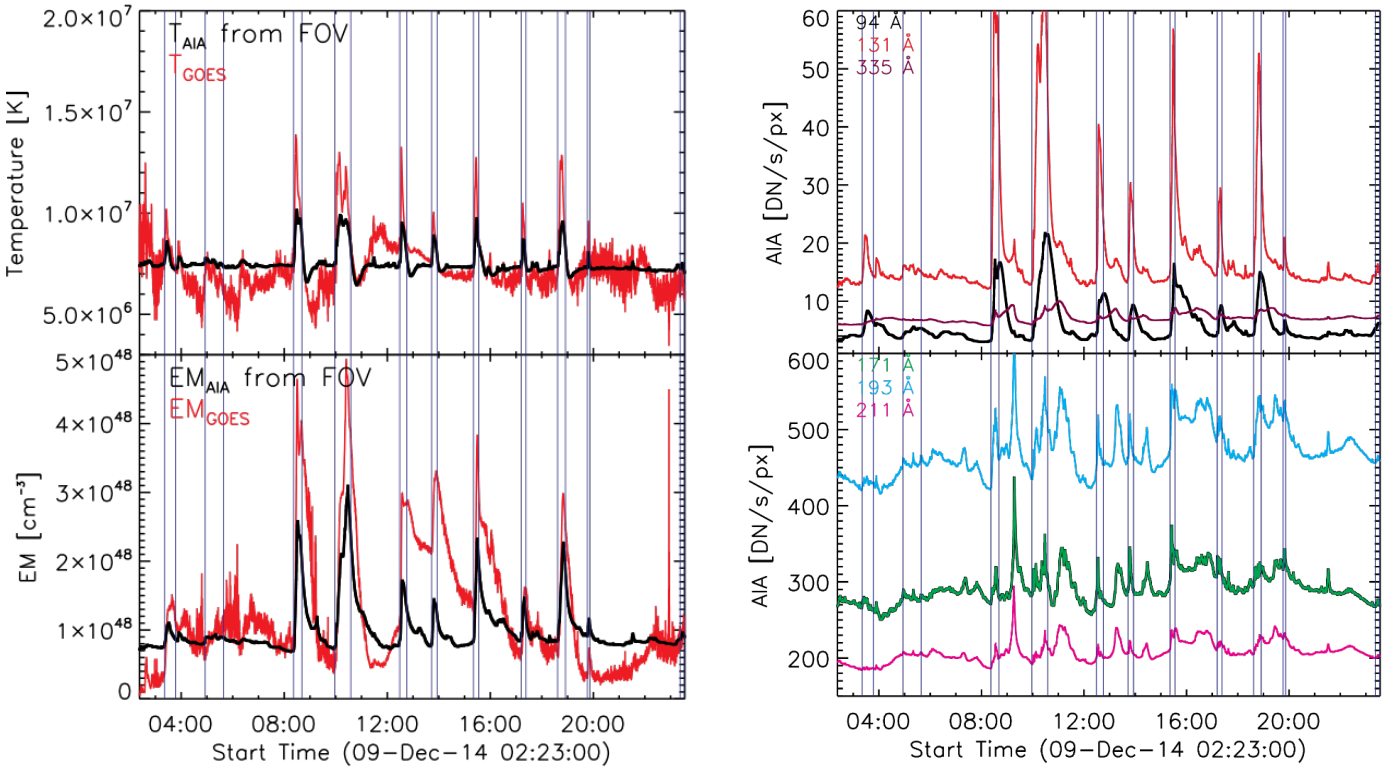
Temperature [K]
2.0×10^7
1.5×10^7
1.0×10^7
5.0×10^6
T_AIA from FOV
T_GOES
EM [cm^-3]
5×10^48
4×10^48
3×10^48
2×10^48
1×10^48
0
EM_AIA from FOV
EM_GOES
04:00
08:00
12:00
16:00
20:00
Start Time (09-Dec-14 02:23:00)
AIA [DN/s/px]
60
50
40
30
20
10
94 Å
131 Å
335 Å
600
500
400
300
200
171 Å
193 Å
211 Å
04:00
08:00
12:00
16:00
20:00
Start Time (09-Dec-14 02:23:00)

Fig. 7.